PCCP

Accepted Manuscript

ROYAL SOCIETY OF CHEMISTRY

www.rsc.org/pccp

PCCP

COMMUNICATION

Conformational ensemble of human α-synuclein physiological form predicted by molecular simulations

Received 00th January 20xx,
Accepted 00th January 20xx

DOI: 10.1039/x0xx00000x

www.rsc.org/pccp

G. Rossetti,[a,b,c,‡] F. Musiani,[a,d,e,‡] E. Abad,[a,f,‡] D. Dibenedetto,[f] H. Mouhib,[g] C.O Fernandez,[h,i] and P. Carloni*[a,f]

We perform here enhanced sampling simulations of N-terminally acetylated human α-synuclein, an intrinsically disordered protein involved in Parkinson's disease. The calculations, consistent with experiments, suggest that the post-translational modification leads to the formation of a transient amphipathic α-helix. The latter, absent in the non-physiological form, alters protein dynamics at the N-terminal and intramolecular interactions.

Parkinson's disease (PD) is the second most common neurodegenerative disease, affecting approximately four million people worldwide.[1] Currently, there is no cure for it. The human protein α-synuclein[2] represents the major component of PD's pathologic proteinaceous deposits in the *substantia nigra* of human brains ('Lewy bodies' and 'Lewy neuritis').[3] Although it remains unclear how α-synuclein initiates neuronal death, there is growing evidence that supports a role for α-synuclein aggregation in the pathological effects associated to PD. The aggregation pathway of α-synuclein represents then an obvious target for therapeutic intervention in PD.[4, 5] The precise function of α-synuclein is unknown, as are the mechanism(s) underlying the structural transition from the innocuous, monomeric disordered conformations of α-synuclein to its neurotoxic forms. Recently, abundant evidence revealed that the monomeric state of α-synuclein undergoes N-terminal acetylation *in vivo* (AcAS, hereafter),[5-7] which differs structurally in a small but subtle way from the widely studied, non-acetylated, non-physiological form (no-AcAS),[5, 6] expressed in *E. coli* and lacking the post-translational modification. Indeed, AcAS' hydrodynamic radius is larger by 0.5 Å than that of no-AcAS. In addition, its N-terminus has higher α-helical propensity.[5-8] Consistently, the chemical shifts of that region show the largest differences between the AcAS and no-AcAS states.[9]

While the structural determinants of no-AcAS' structural ensemble in aqueous solution have been well characterized by NMR measurements,[10-13] those of the physiological form have been explored only in the past few years.[9, 12]

Recently, some of us performed molecular dynamics (MD) simulations of no-AcAS[14] based on the Amber ff99SB force fields[15] with ILDN modification.[16] The calculations, based on the available structural information,[10] turned out to reproduce the available biophysical data, including NMR chemical shifts (CSs)[17-19] and residual dipolar couplings.[20] Prompted by the consistency between these simulations and experimental data, we have used here a MD enhanced sampling method based on the same force field to provide insights into the conformational ensemble of the physiological AcAS form. The predictive power of our simulations is here assessed via an extensive comparison with experimental data, that includes CSs, Circular Dichroism (CD),[7] and measured hydrodynamic radii (RH).[7] Comparison is also made with the reported electrostatic compaction factor, as derived by translational diffusion experiments.[7]

4,000 no-AcAS NMR structures[10] were clustered in six representatives, covering almost three quarters of the protein's conformations, as in ref. [21]. One acetyl group was manually added to the N-terminus of each representative. Each representative was inserted in a water box using a 10 Å buffer zone of solvent around any atom of the protein. The Amber ff99SB force fields[15] with ILDN modification[16] and the TIP3P water model[22] were used for the protein and for the solvent, respectively. The systems were neutralized by adding

[a] Computational Biomedicine, Institute for Advanced Simulation IAS-5 and Institute of Neuroscience and Medicine INM-9, Forschungszentrum Jülich, 52425 Jülich, Germany. E-mail: p.carloni@fz-juelich.de.
[b] Jülich Supercomputing Centre, Forschungszentrum Jülich, 52425 Jülich, Germany.
[c] Department of Oncology, Hematology and Stem Cell Transplantation, RWTH Aachen University, Aachen, Germany.
[d] Scuola Internazionale Superiore di Studi Avanzati (SISSA/ISAS), via Bonomea 265, 34136 Trieste, Italy.
[e] Laboratory of Bioinorganic Chemistry, Department of Pharmacy and Biotechnology, University of Bologna, 40127 Bologna, Italy.
[f] German Research School for Simulation Sciences, Forschungszentrum Jülich, 52425 Jülich, Germany
[g] Institute of Physical Chemistry, RWTH Aachen University, Landoltweg 2, 52056 Aachen, Germany.
[h] Max Planck Laboratory for Structural Biology, Chemistry and Molecular Biophysics of Rosario (MPLbioR), Universidad Nacional de Rosario, 27 de Febrero 210 bis; S2002LRK-Rosario, Argentina.
[i] Institute for drug discovery of Rosario (IIDEFAR), Universidad Nacional de Rosario, Rosario, 27 de Febrero 210 bis; S2002LRK-Rosario, Argentina.
‡ These authors contributed equally to this work.

10 Na^+ ions. Periodic boundary conditions were applied. Electrostatic interactions were calculated using the Particle Mesh-Ewald (PME) method.[23] All bond lengths were constrained by the LINCS algorithm[24] and an integration step of 2 fs was set for all of the MD calculations. Constant temperature and pressure conditions were achieved by coupling the system with a Nosé-Hoover thermostat[25, 26] and an Andersen-Parrinello-Rahman barostat.[27] The systems were geometry-optimized and then equilibrated at 300 K and 1 atm by performing 1 ns of MD-based annealing and 1 ns of constant temperature MD. Next, each representative underwent the replica exchange with solute tempering (REST2)[28, 29] enhanced sampling method at room conditions. For each REST2 simulation, 32 replicas were generated in the temperature range from 300 to 500 K (see SI). Therefore, a total of six 15 ns long independent REST2 simulations were generated. To test the convergence of our simulations we follow the same approach of Wise-Scira and co-workers[30, 31] (see the SI for further details). The molecular simulations were carried out using the GROMACS 4.5.5 program package.[32] The obtained geometries were clustered using the algorithm proposed in ref. [33] with a RMSD cut-off of 2.2 Å with the *g_cluster* tool in GROMACS 4.5.5.[32]

The six lowest temperature replica trajectories were cumulated into a single trajectory to increase the statistic of our conformational ensemble. From the resulting cumulative trajectory, we calculated several properties: (*i*) CSs and CD spectra, using the SHIFTX[34] and the DichroCalc codes,[35] respectively; (*ii*) RH, gyration radii (R_g), and compaction factors (C_F).[36, 37] RH was obtained from a linear fit between R_g and RH from Ref. [36]; we have considered the same linear fit applies for no-AcAS and AcAS, since all the synuclein family exhibit very similar relationship between R_g and RH.[36] R_g was calculated with the *g_gyrate* tool in GROMACS 4.5.5. The C_F were calculated accordingly to ref. [37]. (*iii*) The rigid block analysis was performed as in ref. [38, 39]. The quality factor was calculated for each case as in ref. [38]. (*iv*) Contact maps, hydrogen bonds (HBs) and saltbridges (SBs) were calculated with the *g_mdmap, g_hbonds*, and *g_dist* GROMACS 4.5.5[32] tools, respectively.

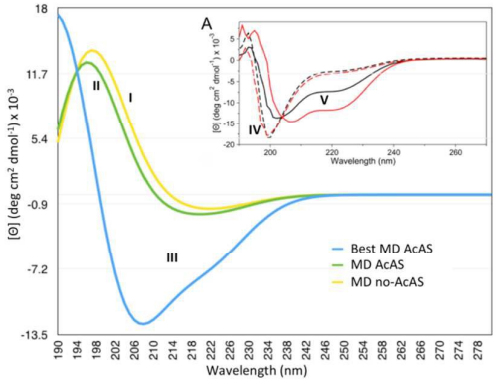

Figure 1. Calculated CD spectra[14] of the predicted conformational ensemble of no-AcAS (**I**), AcAS (**II**) and the structure with the best CSs agreement for the first twelve residues of AcAS (**III**) in Fig. 5B. Inset: Experimental CD spectrum for no-AcAS (black) and AcAS (red) in water (**IV**) and in the presence of 75:1 lipid: protein molar ratio (**V**). Figure adapted from ref. [7].

The calculated CD spectra shift mildly toward α-helical frequencies upon acetylation, similar to what observed in experiments, (Fig. 1).[7] Notably, the structure featuring the best agreement with the CSs shows a clear α-helical signal, with signature negative intensities at 208 and 222 nm. These features were also observed experimentally when AcAS samples were exposed to lipids, which facilitates the formation of helical structures.[7]

Table 1. R_g and RH values of no-AS' and AcAS' predicted conformational ensembles. In parenthesis we report the correspondent values for no-AcAS' and AcAS' most populated cluster.[21] The available experimental values (exp) are also reported. See note 1 for the determination of the error.

	no-AcAS (best ensemble)	AcAS (best ensemble)
R_g	26.4 ± 7 (24.8) Å	27.2 ± 8 Å (20.2)
R_g (exp)	24.7± 5 Å[40]	-
RH	28.8 ± 9 (28.9) Å	29.0 ± 10 (25.7)
RH (exp)	28.2 ± 0.3 [41] Å	28.7 Å [7]

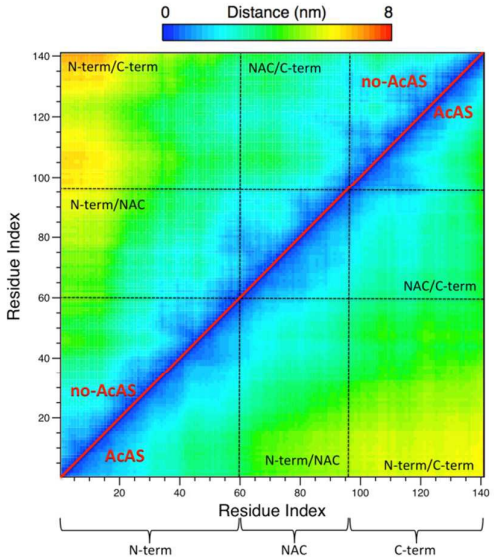

Figure 2. Contact maps for no-AcAS and AcAS, which report the smallest distance between residue pairs. The area of the map corresponding to interdomain interacting regions are highlighted with dotted lines and labeled.

The gyration (R_g) and hydrodynamic (RH) radii decrease upon deacetylation (Tab. 1), consistently with the experimentally observed increase in the global compaction of the protein.[7] The values of RH and R_g compare well with experiments (RH: 28.2 and 28.7 Å for no-AcAS and AcAS, respectively), although the increase of the gyration radius due to acetylation is underestimated (0.2 Å in this work versus 0.5 Å in experiments).[36]

The calculated C_F, that ranges between 0 (random coil) to 1 (folded structure)[37] decreases from 0.53 for no-AcAS to 0.47 for AcAS, also consistent with experimental evidence.[12] The decrease of compaction is associated with a slight decrease of intramolecular interactions: the contact maps of the two

proteins point to a modest decrease of N-terminal/C-terminal and NAC/C-terminal interactions (Fig. 2). Specifically, an overall loss of interdomain SBs (Fig. 3A-C) and a moderate loss of HBs (Fig. 3B) are observed. The Asp2-Lys6 SB interaction is however more persistent in the acetylated variant, possibly because of the increase of α-helicity at the N-terminus,[5, 7] which stabilizes these two residues in an apt conformation for the SB interaction. Interestingly, the intermolecular interactions involving the amino acids undergoing the three familial pathogenic mutations in Parkinson's' (A30P, E46K, and A53T)[42-44] are affected by acetylation due to the looseness of SBs in such region upon acetylation.

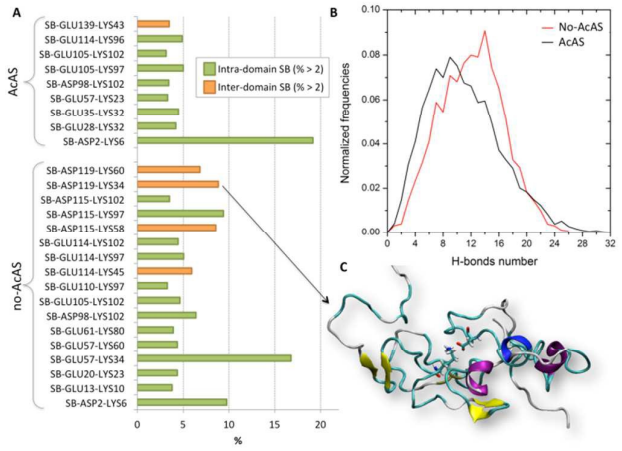

Figure 3. (**A**) SBs occurrence for no-AcAS and AcAS. Interdomain SBs are in red, the intra-domain ones are in green. Only the SBs with occurrence > 2% are reported. (**B**) Average HB distribution for AcAS (black) and no-AcAS (red), normalized over the simulations times. (**C**) Details of no-AcAS structure where inter domain SB is formed.

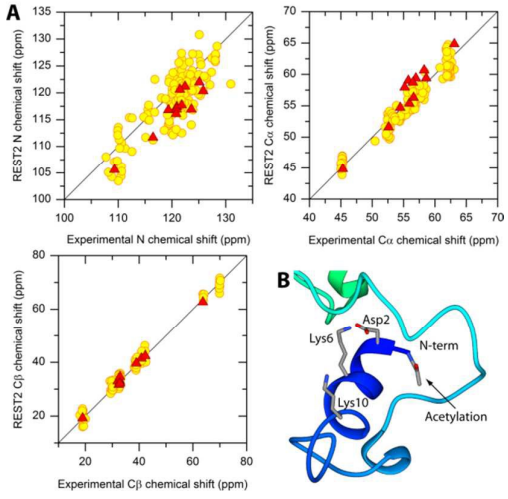

Figure 4. (A) Correlation between experimental[9] and calculated CSs for the entire protein (yellow circles) and for the first twelve residues (red triangles). (**B**) Structure with the best CSs agreement for the first twelve residues of AcAS. The protein is represented in a ribbon scheme and it is colored from blue in the proximity of the N-terminal to red at the C-terminus. The acetyl group at the N-terminal and charged residues mentioned in the text are reported as sticks.

Novel information is obtained on the conformation of the amino acids in the N-terminal region of AcAS. The Pearson's correlation coefficient (CC) between calculated and experimental CSs is 0.86 (Fig. 4A).[9] However, it is as high as 0.94 (Fig. 4A) for residues at the N-term (residues 1 to 12). Residues 2-8 form the α-helix (Fig. 4B) with charged residues (Asp2, Lys6, and Lys10) on one side of the helix and hydrophobic residues (Met1, Val3, Phe4, Met5, Gly7, and Leu8) on the other side (Fig. 4B). The helix is thus amphipathic. Similar conclusions are obtained by NMR studies, which localize the helix between residues 1-9[7] or 1-12[5] of AcAS. The helix may be formed because of favourable electrostatic interactions between the α-helix dipole moment and the acetylated moiety[45, 46] and the consequent formation of backbone

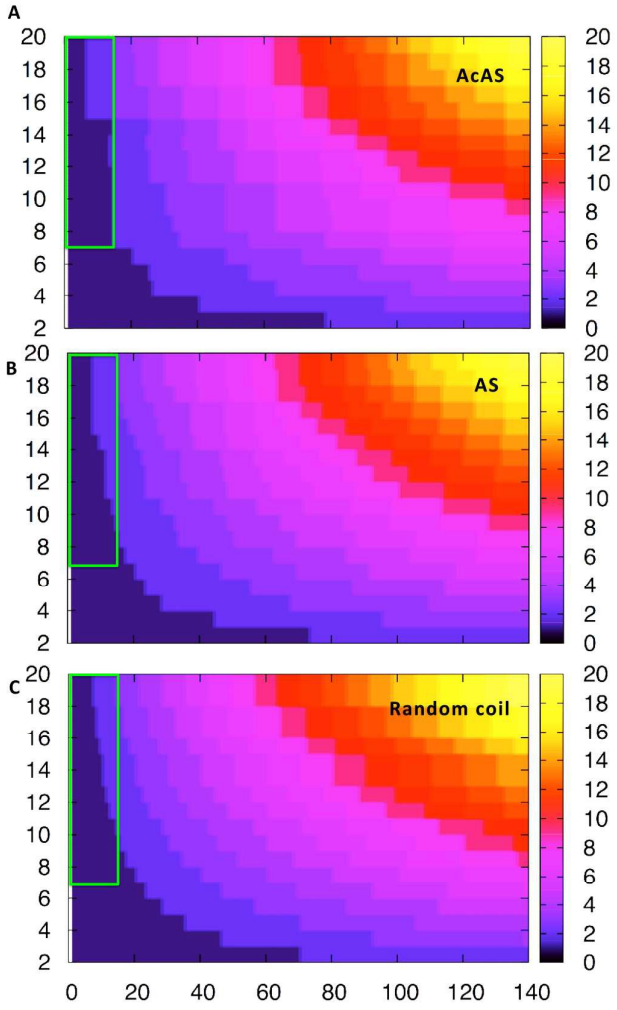

Figure 5. Rigid domain decomposition of (**A**) AcAS, (**B**) no-AcAS, and (**C**) random coil. Each colored fragment corresponds to a rigid domain. Rigid block at N-terminus is highlighted in green (see text).

hydrogen bonding interactions.[45, 46] Consistently with the NMR studies, 15% of AcAS conformations exhibit a α-helix in the first twelve residues of the N-term (see Fig. 4B as an example). These features are not observed in the no-AcAS form of the

protein, and are consistent with the ability of AcAS to bind cellular membranes with an affinity for the lipids ~2-fold stronger with respect to no-AcAS.[7] Indeed, this distinct increase in lipid affinity upon acetylation was shown to depend on the role played by the first 12 residues in initiating membrane binding.[7] Specifically, the preformation of helical structure at the N-terminus significantly increase the rate of binding of AcAS to lipids,[7] a kinetic change that results in the increased lipid binding affinity.[7] The presence of an amphipathic helix further supports the 'initiation-elongation' model of membrane binding: amphipathic helices act as membrane binding anchors for several other proteins.[47-49] This is also the case for AcAS.[50]

Does the presence of the N-terminal helix affect proteins mobility? To address this issue, we performed the so-called 'rigid-block analysis'.[38] This detects dynamically independent domains, i.e.: domains that move in a concerted motion, preserving the shape, but uncorrelated with the rest of the protein. The N-terminus (residues 1-12) of AcAS behaves as a dynamically independent domain, possibly because of the presence of the helix (Fig. 5A). This is not the case for no-AcAS (Fig. 5B), where the removal of the acetyl group is restricted to the correlation of motion to residues 1-6 only. Consistently, the calculated spread of the Φ and Ψ Ramachandran angles of residues 1-12 decreases upon acetylation and, expectedly, they are compatible with those of a helix (Fig. 6).

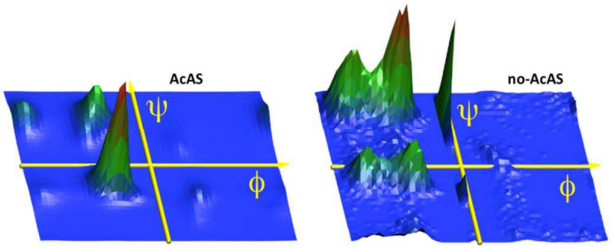

Figure 6. Ramachandran plots of the first 12 residues for AcAS (left) and no-AcAS (right).

The rest of the protein moves in a uncorrelated way in both proteins, consistently with the same NMR properties of residues 13-140.[7] in detail, the domain decomposition in no-AcAS is more similar to a random coil than AcAS. Thus, residues in no-AcAS move in a less correlated way than AcAS ones, closer to the behavior of a random coil and consistent with a decrease of secondary structure on passing from AcAS to no-AcAS (29% and 25%, respectively).

In conclusion, our molecular modeling study - as demonstrated by NMR,[5, 9] CD,[7] and translational diffusion experiments[7] – suggests that, upon acetylation, α-synuclein adopt a broken amphipathic helix conformation at the N-terminal. On one hand this confers more rigidity to the N-terminal domain; Consistently, the change in AcAS fibrillation rate observed in experiments upon acetylation was suggested to depend on the stabilization of the N-terminal region of the protein.[5] On the other hand, it causes a loss of HBs and SBs interactions, decreasing the compactness of the protein and affecting the intermolecular interaction of relevant regions for aggregation. Using NMR chemical shifts and fluorescence experiments, Kang and co-workers indeed showed that secondary structural propensity in residues 5–8, 14–31, and 50–57 are highly correlated to fibril growth rate.[5] 14–31, and 50–57 are the regions in which we observe loss of SBs. Therefore, our calculations support Kang and co-workers' idea that N-terminal acetylation inhibits the formation of the "fibrillation promoting" transient helix at residues 14–31 and 50–57, while stabilizing the formation of the "fibrillation inhibiting" transient helix in residues 1–12, thereby resulting in slower fibrillation rates relative to the no-AcAS."

Acknowledgements

This work was financially supported by the Deutsche Forschungsgemeinschaft (DFG) under project (CA 973/14-1). FM was financed by Programma Operativo del Fondo Sociale Europeo 2007/2013 of Regione Autonoma Friuli Venezia Giulia and by CIRMMP (Consorzio Interuniversitario di Risonanze Magnetiche di Metallo-Proteine). This project was granted 270,000 core hours on the JUROPA supercomputer in the Jülich Supercomputing Centre through the NIC program (NIC: 5720 and 6695).

Notes and references

Note 1. The reported error on Rg is the standard deviation of the gyration radius measurements along the entire trajectory. It might be rather large because of the large conformational diversity of an IDP such as α-synuclein. The theoretical RH error was obtained by propagation from Rg error. For experiments, RH errors come from the measurement of diffusion coefficients,[41] using the Stokes-Einstein-Sutherland equation. The error reported in those cases is the error in the experimental measurement, which has nothing to do with the error associated with conformational diversity of the protein.

1. L. M. L. de Lau and M. M. B. Breteler, *The Lancet Neurology*, 2006, **5**, 525-535.
2. K. A. Jellinger, *Mov. Disors.*, 2003, **18 supl 6**, S2-S12.
3. T. M. Dawson and V. L. Dawson, *J. Clin. Invest.*, 2003, **111**, 145-151.
4. G. M. Moriarty, M. K. Janowska, L. Kang and J. Baum, *FEBS Lett.*, 2013, DOI: papers2://publication/uuid/80EB2EE6-A735-4ACC-80ED-12802A5C6E59.
5. L. Kang, G. M. Moriarty, L. A. Woods, A. E. Ashcroft, S. E. Radford and J. Baum, *Protein sci.*, 2012, **21**, 911-917.
6. A. J. Trexler and E. Rhoades, *Protein sci.*, 2012, **21**, 601-605.
7. A. S. Maltsev, J. Ying and A. Bax, *Biochemistry*, 2012, **51**, 5004-5013.
8. B. Fauvet, M.-B. Fares, F. Samuel, I. Dikiy, A. Tandon, D. Eliezer and H. A. Lashuel, *J. Biol. Chem.*, 2012, **287**, 28243-28262.
9. J. Roche, J. Ying, A. S. Maltsev and A. Bax, *ChemBioChem*, 2013, **14**, 1754-1761.
10. M. M. Dedmon, K. Lindorff-Larsen, J. Christodoulou, M. Vendruscolo and C. M. Dobson, *J Am Chem Soc*, 2004, **127**, 476-477.
11. H.-Y. Kim, H. Heise, C. O. Fernández, M. Baldus and M. Zweckstetter, *ChemBioChem*, 2007, **8**, 1671-1674.
12. C. W. Bertoncini, Y.-S. Jung, C. O. Fernández, W. Hoyer, C. Griesinger, T. M. Jovin and M. Zweckstetter, *Proceedings of the National Academy of Sciences*, 2005, **102**, 1430-1435.

13. M.-K. Cho, G. Nodet, H.-Y. Kim, M. R. Jensen, P. Bernadó, C. O. Fernández, S. Becker, M. Blackledge and M. Zweckstetter, *Protein Science*, 2009, **18**, 1840-1846.
14. D. Dibenedetto, G. Rossetti, R. Caliandro and P. Carloni, *Biochemistry*, 2013, **52**, 6672-6683.
15. V. Hornak, R. Abel, A. Okur, B. Strockbine, A. Roitberg and C. Simmerling, *Proteins*, 2006, **65**, 712-725.
16. K. Lindorff-Larsen, S. Piana, K. Palmo, P. Maragakis, J. L. Klepeis, R. O. Dror and D. E. Shaw, *Proteins*, 2010, **78**, 1950-1958.
17. W. Wang, I. Perovic, J. Chittuluru, A. Kaganovich, L. T. T. Nguyen, J. Liao, J. R. Auclair, D. Johnson, A. Landeru, A. K. Simorellis, S. Ju, M. R. Cookson, F. J. Asturias, J. N. Agar, B. N. Webb, C. Kang, D. Ringe, G. A. Petsko, T. C. Pochapsky and Q. Q. Hoang, *Proceedings of the National Academy of Sciences*, 2011.
18. W. Bermel, I. Bertini, I. C. Felli, Y.-M. Lee, C. Luchinat and R. Pierattelli, *Journal of the American Chemical Society*, 2006, **128**, 3918-3919.
19. J. N. Rao, Y. E. Kim, L. S. Park and T. S. Ulmer, *Journal of Molecular Biology*, 2009, **390**, 516-529.
20. T. Gurry, O. Ullman, C. K. Fisher, I. Perovic, T. Pochapsky and C. M. Stultz, *Journal of the American Chemical Society*, 2013, **135**, 3865-3872.
21. V. Losasso, A. Pietropaolo, C. Zannoni, S. Gustincich and P. Carloni, *Biochemistry*, 2011, **50**, 6994-7001.
22. W. Jorgensen, J. Chandrasekhar, J. Madura, R. Impey and M. Klein, *J Chem Phys*, 1983, **79**, 926-935.
23. T. Darden, D. York and L. Pedersen, *J. Chem. Phys.*, 1993, **98**, 10089-10092.
24. B. Hess, H. Bekker, H. J. C. Berendsen and J. G. E. M. Fraaije, *J. Comput. Chem.*, 1997, **18**, 1463-1472.
25. S. Nose, *Journal of Chemical Physics*, 1984, **81**, 511-519.
26. W. G. Hoover, *Phys. Rev., A*, 1985, **31**, 1695-1697.
27. M. Parrinello and A. Rahman, *Journal of Applied physics*, 1981, DOI: papers2://publication/uuid/D718B102-5C97-4408-892F-6454B35D3AAE.
28. L. Wang, R. A. Friesner and B. J. Berne, *J. Phys. Chem. B*, 2011, **115**, 9431-9438.
29. T. Terakawa, T. Kameda and S. Takada, *J. Comput. Chem.*, 2011, **32**, 1228-1234.
30. O. Coskuner and O. Wise-Scira, *ACS Chem. Neurosci.*, 2013, **4**, 1101-1113.
31. O. Coskuner, O. Wise-Scira, G. Perry and T. Kitahara, *ACS Chem. Neurosci.*, 2013, **4**, 310-320.
32. E. Lindahl, B. Hess and D. van der Spoel, *Journal of Molecular Modeling*, 2001, **7**, 306-317-317.
33. X. Daura, K. Gademann, B. Jaun, D. Seebach, W. F. van Gunsteren and A. E. Mark, *Angewandte Chemie International Edition*, 1999, **38**, 236-240.
34. S. Neal, A. M. Nip, H. Zhang and D. S. Wishart, *J Biomol NMR*, 2003, **26**, 215-240.
35. B. M. Bulheller and J. D. Hirst, *Bioinformatics*, 2009, **25**, 539-540.
36. J. R. Allison, R. C. Rivers, J. C. Christodoulou, M. Vendruscolo and C. M. Dobson, *Biochemistry*, 2014, **53**, 7170-7183.
37. D. K. Wilkins, S. B. Grimshaw, V. Receveur, C. M. Dobson, J. A. Jones and L. J. Smith, *Biochemistry*, 1999, **38**, 16424-16431.
38. L. Ponzoni, G. Polles, V. Carnevale and C. Micheletti, *Structure*, 2015, DOI: papers2://publication/doi/10.1016/j.str.2015.05.022.
39. U. von Luxburg, *Statistics and Computing*, 2007, **17**, 395-416.
40. M. M. Dedmon, K. Lindorff-Larsen, J. Christodoulou, M. Vendruscolo and C. M. Dobson, *J Am Chem Soc*, 2005, **127**, 476-477.
41. K. E. Paleologou, A. W. Schmid, C. C. Rospigliosi, H. Y. Kim, G. R. Lamberto, R. A. Fredenburg, P. T. Lansbury, Jr., C. O. Fernandez, D. Eliezer, M. Zweckstetter and H. A. Lashuel, *The Journal of biological chemistry*, 2008, **283**, 16895-16905.
42. M. H. Polymeropoulos, C. Lavedan, E. Leroy, S. E. Ide, A. Dehejia, A. Dutra, B. Pike, H. Root, J. Rubenstein and R. Boyer, *Science*, 1997, **276**, 2045-2047.
43. R. Krüger, W. Kuhn, T. Müller, D. Woitalla, M. Graeber, S. Kösel, H. Przuntek, J. T. Epplen, L. Schols and O. Riess, *Nat Genet*, 1998, **18**, 106-108.
44. J. J. Zarranz, J. Alegre, J. C. Gómez-Esteban, E. Lezcano, R. Ros, I. Ampuero, L. Vidal, J. Hoenicka, O. Rodriguez, B. Atarés, V. Llorens, E. Gomez Tortosa, T. del Ser, D. G. Muñoz and J. G. de Yebenes, *Ann. Neurol.*, 2004, **55**, 164-173.
45. R. Aurora and G. D. Rose, *Protein science : a publication of the Protein Society*, 1998, **7**, 21-38.
46. A. Chakrabartty, A. J. Doig and R. L. Baldwin, *Proc. Natl. Acad. Sci. U.S.A.*, 1993, **90**, 11332-11336.
47. S. S. Y. Chong, S. G. Taneva, J. M. C. Lee and R. B. Cornell, *Biochemistry*, 2014, **53**, 450-461.
48. Y.-L. Shih, K.-F. Huang, H.-M. Lai, J.-H. Liao, C.-S. Lee, C.-M. Chang, H.-M. Mak, C.-W. Hsieh and C.-C. Lin, *journals.plos.org*, **6**, e21425.
49. F. Lu and A. Taghbalout, *Journal of Biological Chemistry*, 2013, **288**, 7241-7251.
50. J. Varkey, J. M. Isas, N. Mizuno, M. B. Jensen, V. K. Bhatia, C. C. Jao, J. Petrlova, J. C. Voss, D. G. Stamou, A. C. Steven and R. Langen, *Journal of Biological Chemistry*, 2010, **285**, 32486-32493.

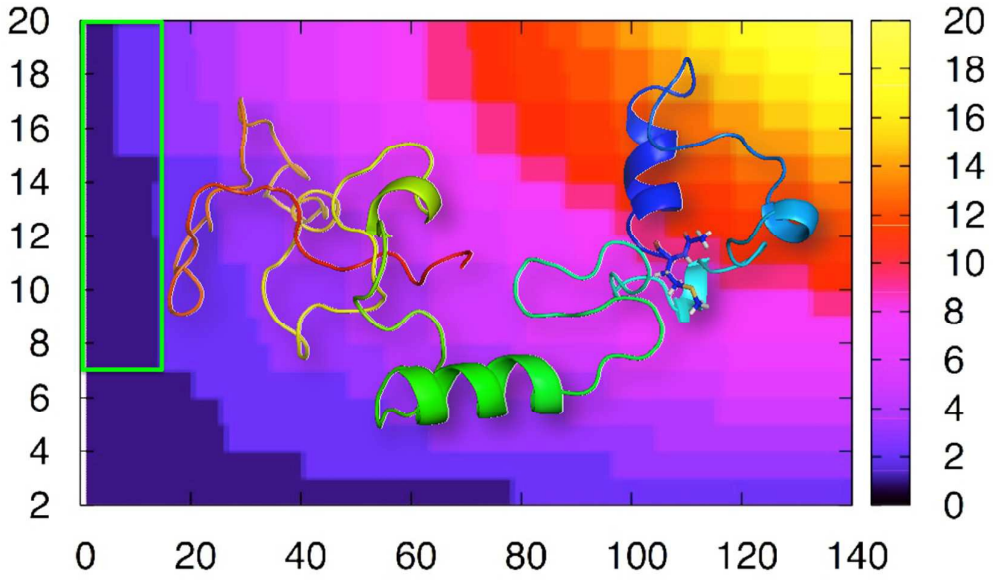

Enhanced sampling simulations of N-terminally acetylated human α-synuclein suggest that the post-translational modification leads to the formation of a transient amphipathic α-helix altering protein dynamics at the N-terminal and intramolecular interactions.